Postprint: Vereecken E, Janssen H, Roels S. 2018. A determination methodology for the spatial profile of the convective heat transfer coefficient on building components. *Indoor and Built Environment 27(4), 512-527*. DOI: 10.1177/1420326X16677330

A DETERMINATION METHODOLOGY FOR THE SPATIAL PRO2016 FILE OF THE CONVECTIVE HEAT TRANSFER COEFFICIENT ON BUILDING COMPONENTS

EVY VEREECKEN[A1], HANS JANSSEN[B] AND STAF ROELS[C]

[A] KU LEUVEN, BUILDING PHYSICS SECTION, KASTEELPARK ARENBERG 40, B-3001 LEUVEN, BELGIUM, +32 16321098

EVY.VEREECKEN@BWK.KULEUVEN.BE

[B]KU LEUVEN, BUILDING PHYSICS SECTION, KASTEELPARK ARENBERG 40, B-3001 LEUVEN, BELGIUM

HANS.JANSSEN@BWK.KULEUVEN.BE

[C] KU LEUVEN, BUILDING PHYSICS SECTION, KASTEELPARK ARENBERG 40, B-3001 LEUVEN, BELGIUM

STAF.ROELS@BWK.KULEUVEN.BE

[1]CORRESPONDING AUTHOR

KEY WORDS:

Local convective heat transfer coefficient, spatial profile, convective heat exchange, Monte Carlo analysis, corner, thermal bridge

Postprint: Vereecken E, Janssen H, Roels S. 2018. A determination methodology for the spatial profile of the convective heat transfer coefficient on building components. *Indoor and Built Environment 27(4), 512-527*. DOI: 10.1177/1420326X16677330

ABSTRACT

Several experimental procedures have been established to determine the convective heat transfer coefficient, a frequently used parameter in many engineering disciplines. Almost all of these methodologies focus on point or spatially averaged values. Yet, in many studies the spatial profile of the local convective heat transfer is of importance. In this paper, a methodology to determine such spatial profile is proposed. In this method, experiments are combined with Monte Carlo simulations. Such an approach makes it possible to account for inaccuracies in the input data. As an example, the methodology is applied to determine the spatial profile of the local convective heat transfer coefficient near a corner for two thermal bridge configurations. The temperature difference between interior surface and indoor air is found to restrict the applicability of the method. Nonetheless, for the case with a sufficient temperature difference, the order of magnitude of the convective heat transfer coefficients further away from the corner is in line with literature data. An important limitation of the technique at this stage of its development is, however, its requirement for prior knowledge of the equation that describes the spatial profile of the convective heat transfer coefficient. Despite these drawbacks, the methodology shows much potential and can be valuable for other applications as well.

Postprint: Vereecken E, Janssen H, Roels S. 2018. A determination methodology for the spatial profile of the convective heat transfer coefficient on building components. *Indoor and Built Environment 27(4), 512-527*. DOI: 10.1177/1420326X16677330

INTRODUCTION

The convective heat transfer coefficient is a frequently used parameter in many engineering applications, such as construction engineering,[1-4] electrical engineering,[5,6] physiological engineering[7,8] and micro-scale engineering,[9] to name only a few. This coefficient, h_c (W/(m^{2}K)), avoids the explicit and often complicated modelling of the momentum, mass and heat exchange between a surface and a zone, because it directly expresses the relationship between the convective heat flux q_c (W/m^2) and the difference between surface temperature T_s (K) and zone temperature T_i (K) as given in equation (1):

$$q_c = h_c(T_i - T_s) \tag{1}$$

Different methodologies for direct or indirect experimental determination of the convective heat transfer coefficient are available and are reviewed below. These methodologies mainly focus on point or spatially averaged values, which are subsequently dominant in the literature.[10-13] However, more precise spatial profiles of the local convective heat transfer coefficient are often required to allow accurate simulations.

This paper presents a methodology for the determination of the spatial profile of the interior convective heat transfer coefficient in buildings. The spatial profile of the interior convective heat transfer coefficient is of crucial importance as it can have a

significant influence in energy simulations[14] and in mould growth assessments,[15,16] of which the latter are of importance for occupant health and material degradation related issues. Despite its importance, previous studies on the convective heat transfer coefficient on building components are mainly performed on isolated free-edge surfaces,[17-19] hence resulting in coefficients that are actually inappropriate for surfaces in real buildings. Efforts to solve the latter shortcoming can be found in more recent studies focusing on the convective heat transfer coefficient for surfaces in two- and three dimensional enclosures.[20-21] Furthermore, attention has been drawn to the influence of a potential scale effect,[20] and hence measurements on real-size building enclosures with realistic boundary conditions are preferred to obtain realistic convective heat transfer coefficients.[22]

Notwithstanding these efforts to increase the reliability of measurements on convective heat transfer coefficients, the determination of the spatial profile of the local convective heat transfer coefficient has received little attention so far. This results in a scarcity of studies applying such a spatial profile,[23] even though its use is desirable to achieve an accurate determination of, for instance, the local surface temperature near a corner. A determination methodology to achieve this spatial profile is hence required. In this respect, an important study was performed within the framework of the IEA ECBCS Annex 14-project,[10,24] in which the heat transfer coefficient near edges and corners has been studied based on a test corner in the

laboratory. This corner configuration together with the material's thermal conductivity and the measured surface temperatures were used as an input to a computer program to calculate the heat flux distribution. The division of the local heat fluxes and the difference between the reference and local surface temperatures yielded a spatial profile of the total heat transfer coefficient, which was afterwards split into a radiative and convective part. A closer look at the study indicates though that the outcomes achieved for the convective heat transfer coefficients near the corner disagree with the common physical expectations, given that the study indicated an increase of the convective heat transfer coefficient towards the corner. Possibly, small inaccuracies in certain measurements such as surface temperatures, especially near the corner, may have had a significant impact in the calculation, and thus may lie at the root of these seemingly erroneous results.

The methodology described in the current paper combines experimental measurement and numerical interpretation to determine a spatial profile for the local convective heat transfer coefficient. The Monte Carlo analysis takes into account a spread on the input due to potential noise in the measurement data.

The current paper focuses on the convective part of the heat transfer, while including radiation in total heat exchange. An accurate implementation of the total heat exchange is important for the determination of, for instance, the local surface temperature. Separate implementations of convection and radiation are, however,

preferable since these two types of heat exchange represent different physical phenomena. Presently, such separation is already applied in many building simulation models.[25,26] For the radiative part, this implies a rather straightforward implementation of the radiative heat exchange between subsections of surfaces at different temperatures.[27] The implementation of the convective heat transfer remains challenging though, especially for local phenomena.[28-31]

BRIEF LITERATURE REVIEW

This section gives an overview of the main methodologies currently applied in several engineering applications to determine the convective heat transfer coefficient. Experimental as well as numerical methodologies are available. As a consequence of the increasing computational power, computational fluid dynamics (CFD) based techniques have become progressively more popular.[32-35] The overview in the current paper, however, focuses on experimental procedures. Full-scale[2,22,36,37] or wind-tunnel experiments[38,39] can be distinguished. The main experimental methodologies can be subdivided into (1) mass transfer methodologies, (2) stationary heat balance methodologies and (3) transient heat transfer methodologies.

Mass transfer methodologies

In mass transfer methodologies, the moisture transfer coefficient is measured. This coefficient can be converted to the convective heat transfer coefficient by means of

the heat and mass analogy.[40] The best known mass transfer method is the naphthalene sublimation technique,[41,42] although other mass transfer methods can also be found.[43] In the naphthalene method, naphthalene, which sublimates at room temperature, is applied to the test setup. Based on the change in weight of small pieces of naphthalene obtained during a specified measurement period, the mass transfer rate from each investigated surface can be calculated. Another possibility is to measure the sublimation depth or the time needed for a thin film of naphthalene sprayed on a transparent substrate to vanish.[44,45,46]. This makes the determination of the local mass transfer coefficient possible.

A disadvantage of the naphthalene sublimation technique is its high sensitivity to the surface temperature[41,45]. Furthermore, Mendes[41] mentioned the difficulty to control the naphthalene sublimation technique for natural convection experiments, resulting in poor repeatability. More importantly, the heat and mass analogy is not always valid for interior boundary conditions.[47] On the other hand, since a conversion of the moisture transfer coefficient by the use of heat and mass analogy immediately results in the convective heat transfer coefficient, no correction for radiation is required.

Stationary heat balance methodologies

Another type of methodology frequently applied to calculate the convective heat transfer coefficient at building components makes use of the stationary heat balance equation.[22,37,48] In this approach, the convective heat flux is derived from the total

heat flux by correcting for the radiative part (Appendix 1). Next, the convective heat flow is divided by the temperature difference between surface and air to come to the convective heat transfer coefficient.

The total heat flux in this approach can be obtained via a heat flux sensor. Such rather direct methodology induces a number of drawbacks though. Indeed, heat flux sensors are rather expensive and their disturbance of the air flow is, moreover, detrimental to the measurement's reliability. These drawbacks have therefore led to modified methodologies by making use of flux meters embedded in the test setup or even avoiding flux meters. An example of such a modified methodology is the heated plate method.[1,20,36] In this method, a heated test panel is attached to the investigated surface. Loveday and Taki,[36] for instance, used a test panel composed of a heater mat sandwiched between an aluminium plate and an internal copper plate, which provided a uniform heat flow for detection by a heat flux meter with which it was in contact. The heat flux meter, in turn, was shielded with an external copper plate. The implementation of a heat flow meter can, however, be avoided by measuring the power input to the plates.[20,49]

Although frequently applied, the heated plate method does not provide suitable results for real buildings.[50] A similar method can, however, be applied without a heated plate. Khalifa and Marchall,[51] for instance, used a second zone to control the exterior surface temperature of a vertical wall of the real test zone and used the wall

material itself as a heat flux meter. Also, Wallentén[22] used a similar calculation method, though based on the conductive – and thus total – heat flow through a real building element with known thermal conductivity instead of through a heated plate. For a one-dimensional wall assembly, this method can be applied rather easily. The interior and exterior surface temperatures can be measured. Thus, with the thermal conductivity of the wall elements known, the conductive heat flow through the wall, q_{cond} (W/m²), can be determined as defined by equation (2):

$$q_{cond} = \frac{T_{se} - T_{si}}{R_{wall}} \tag{2}$$

where $T_{se/si}$ is the exterior/interior surface temperature (K) and R_{wall} is the total thermal resistance of the wall ((m²K)/W). Next, the interior convective heat flow q_c (W/m²) can be obtained by equation (3) by subtracting the radiative heat flux q_r (W/m²) (see Appendix 1) from q_{cond} (W/m²):

$$q_c = q_{cond} - q_r \tag{3}$$

Finally, by measuring the indoor air temperature T_i (K), the interior convective heat transfer coefficient h_{ci} (W/(m²K)) can be calculated as given in equation (4):

$$h_{ci} = \frac{q_c}{T_{si} - T_i} \quad (4)$$

A similar calculation can be performed for the exterior convective heat transfer coefficient. In that case though, short-wave radiation should be considered or nocturnal measurements should be used.

Whereas the methodology without heating plates is more in line with a real-life situation, it has drawbacks. Although a simple analytical calculation will suffice to solve the heat balance for a one-dimensional problem, calculating the spatial distribution of the heat transfer coefficient based on the heat balance approach is rather complicated. In-house experience indicates, for example, that small uncertainties in the temperature measurement can result in physically unrealistic results and even a numerically indeterminate problem.

In addition to the methodologies mentioned above, some studies suggest the measurement of the surface temperature profiles in the near-wall boundary layer to deduce the convective heat transfer coefficient.[50,52,53] These studies were based on the measurement procedure originally developed by Mayer, in which a 'Mayer ladder' is applied to measure the temperature profile from the (wall) surface to the air.[52] Based on this profile, the thickness d (m) of the thermal boundary layer can be determined, which in turn defines the convective heat transfer h_c (W/(m^{2}K)) by equation (5):

$$h_c = \frac{\lambda_{air}}{d} \quad (5)$$

with λ_{air} the thermal conductivity of air (W/(mK)). A determination of the spatial profile based on this principle is, however, complex.

Transient heat transfer methodologies

Transient methodologies are firmly established as well.[54] In these methodologies, the temporal evolution of the surface temperature is observed and combined with the solution of the transient conduction equation. Conventionally, a step-change in air temperature is imposed as boundary condition.[55] This is often difficult to achieve though. Therefore, Newton et al.[56] proposed an exponential-series technique to represent the rise in air temperature in 'slow transient' experiments. The surface temperature is often measured with thermochromic liquid crystals[49,57-60], which display colours whose wavelengths are proportional to temperature.

The transient methodologies as currently applied do, however, neglect potential inaccuracies associated with the measured temperatures and the material properties, which can bring about significant uncertainties to the calculated heat transfer coefficient.[61,62]

Postprint: Vereecken E, Janssen H, Roels S. 2018. A determination methodology for the spatial profile of the convective heat transfer coefficient on building components. *Indoor and Built Environment 27(4), 512-527*. DOI: 10.1177/1420326X16677330

PROPOSED NOVEL METHODOLOGY

General principle

For the determination of the spatial profile of the local convective heat transfer coefficient, using the methodologies mentioned in the previous section is difficult or even impractical. In the current study, a novel procedure that allows determination of such a spatial profile is presented. This procedure combines experimental measurements and numerical analysis and is based on the 'heat balance method'. A schematic overview of the methodology is given in Figure 1.

In the experimental part, the exterior surface of a wall construction was exposed to a specific surface temperature. Inside the test room, heating ensured a specific air temperature. After achieving steady-state conditions, the spatial temperature profile at the interior surface was measured. Based on these data, the spatial interior convective heat transfer coefficient was determined. To this end, the measurements were compared to simulations. Because of the two- (or three-) dimensional nature of the configuration, the analytical determination approach was replaced by a numerical analysis simulating the heat transport in the construction. Furthermore, instead of a single calculation, a Monte Carlo analysis was performed. In this way, the problem was solved inversely.

Postprint: Vereecken E, Janssen H, Roels S. 2018. A determination methodology for the spatial profile of the convective heat transfer coefficient on building components. *Indoor and Built Environment 27(4), 512-527*. DOI: 10.1177/1420326X16677330

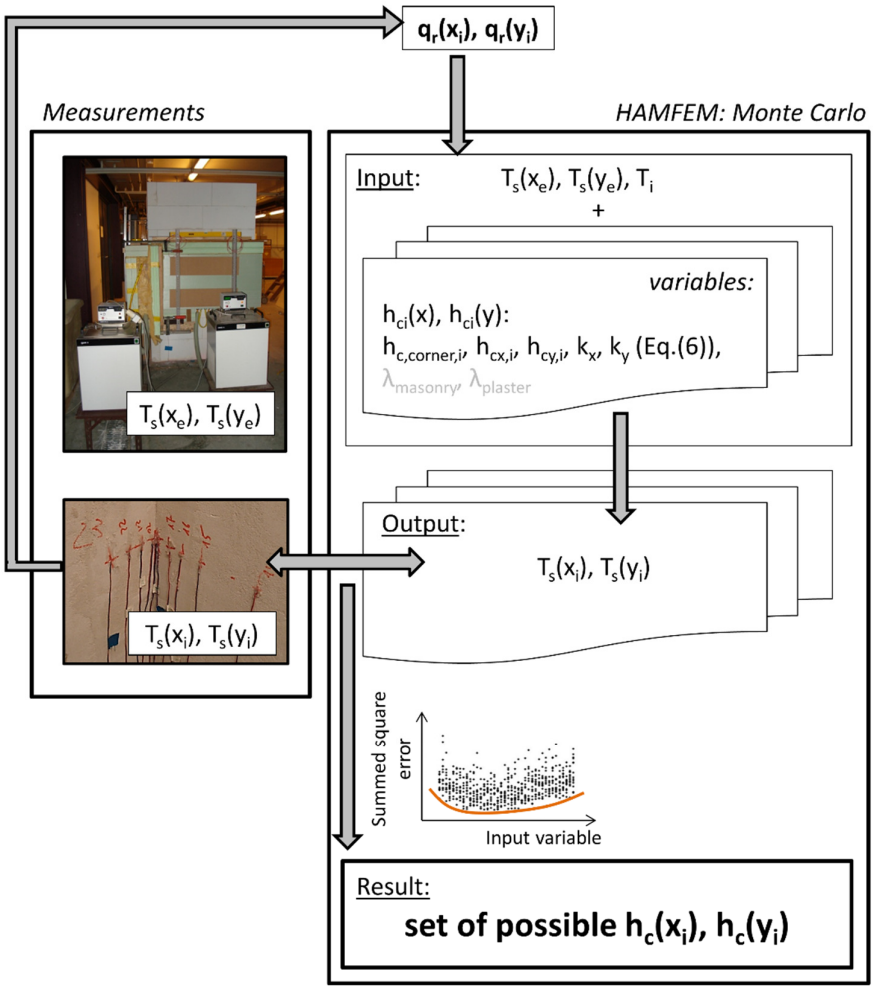

Figure 1. Schematic overview of the determination procedure for the spatial profile of the convective interior heat transfer coefficient.

The main unknown parameters in the Monte Carlo analysis were the spatial profiles of the local convective interior heat transfer coefficient. To achieve the most

appropriate spatial profiles of the local convective interior heat transfer coefficient, the numerically calculated temperature profiles at the interior surface were compared to the experimentally obtained profiles. The interior convective heat transfer coefficient profiles that resulted in the best match between simulated and measured interior surface temperatures were assumed to yield the desired coefficients.

Experimental setup

Test configurations

The spatial profile of the convective heat transfer coefficient near a corner was experimentally investigated for two configurations (see Figure 2):

1) Configuration 1: an uninsulated exterior corner,
2) Configuration 2: a junction between an exterior wall with 6 cm interior insulation and an uninsulated interior wall.

The two wall configurations were investigated to examine the applicability of the proposed methodology, which is important for the validation purpose. A discussion on the thermal performance of the configurations and on the influence of the spatial profile of the convective heat transfer coefficient can be found in Vereecken[65].

To determine the spatial profile of the local convective heat transfer coefficients for the two configurations, a test corner was built in the laboratory. A schematic view of the test setup is shown in Figure 3. The total height of the test corner was 2 metres.

A horizontal masonry strip of 60 cm height was built (Figure 3(a)). Above and below the masonry, cellular concrete was used to act as a good insulation layer. At the interior masonry surface, a lime plaster was applied. To measure the interior surface temperature as a function of the distance from the corner, thermocouples were glued or taped to the surface. After an individual calibration of the thermocouples an accuracy of ±0.1°C was achieved. This accuracy does not take into account potential deviations caused by fixing (e.g. gluing or taping) the thermocouple to the surface. However, as extra attention was paid to proper positioning of the thermocouples we assume that this extra inaccuracy was of minor importance in our test case. For Configuration 1, the position of the different thermocouples is shown in Figure 3. In order to measure the temperature profile near the interior corner in more detail, the distance between the thermocouples was small near the interior corner. As a more one-dimensional heat flow and hence a spatially more constant surface temperature was expected further away from the corner, the thermocouples became more sparsely distributed. For Configuration 2, extra thermocouples were glued on the interior insulation layer. Also for the latter configuration, the thermocouples were clustered near the interior corner after placing interior insulation. The thermocouples were glued at the half height of the masonry layer.

For Configuration 1 (exterior corner), liquid-cooled cold plates were placed at the exterior masonry surfaces to simulate the exterior climate. The cold plates'

temperatures were controlled by two cooling units, one for each wall. Thermocouples were glued to the exterior masonry surface (between the masonry and the liquid-cooled cold plate) to enable accurate control of the cooling units. To avoid cooling of the laboratory space, the liquid-cooled cold plates were covered with insulation at the side of the laboratory (Figure 3(b)). For Configuration 2 (junction between an exterior and an interior wall), a liquid-cooled cold plate was placed on the 31.5 cm thick masonry wall only. On the 21 cm thick masonry wall, an insulation layer was placed at the exterior surface to provide an adiabatic plane at the outer side of this wall. Hence, a test setup of half the junction suffices to study the thermal behaviour of Configuration 2.

Edge effects at the far end of the walls were avoided by an insulation board. To obtain a controlled indoor temperature, a closed environment was built (Figure 3). This also protects the test corner from the influences of the laboratory (e.g., air movements caused by the HVAC installation or by people, radiation exchange between the wall and objects in the laboratory). The indoor temperature was controlled by infrared lamps. A uniform room temperature was obtained by use of two small fans. To avoid the influences of radiation from the infrared lamps and air circulation by the fans on the measurement, the test corner was shielded with two vertical boards and a horizontal board at the top of the construction. In the test room, the air temperature at 0.5 m from the walls was measured by a thermocouple

shielded with tin foil. This thermocouple was positioned at 95 cm above the floor, which was the same height as the position of the thermocouples on the wall surface.

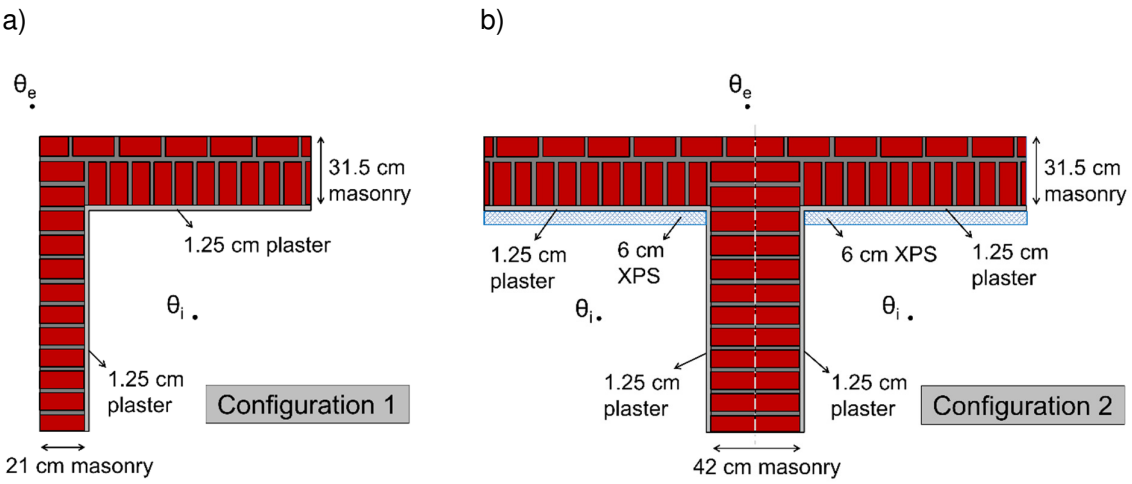

Figure 2. Test configurations: (a) exterior non-insulated wall, (b) junction between insulated exterior wall and non-insulated interior wall.

Postprint: Vereecken E, Janssen H, Roels S. 2018. A determination methodology for the spatial profile of the convective heat transfer coefficient on building components. *Indoor and Built Environment 27(4), 512-527*. DOI: 10.1177/1420326X16677330

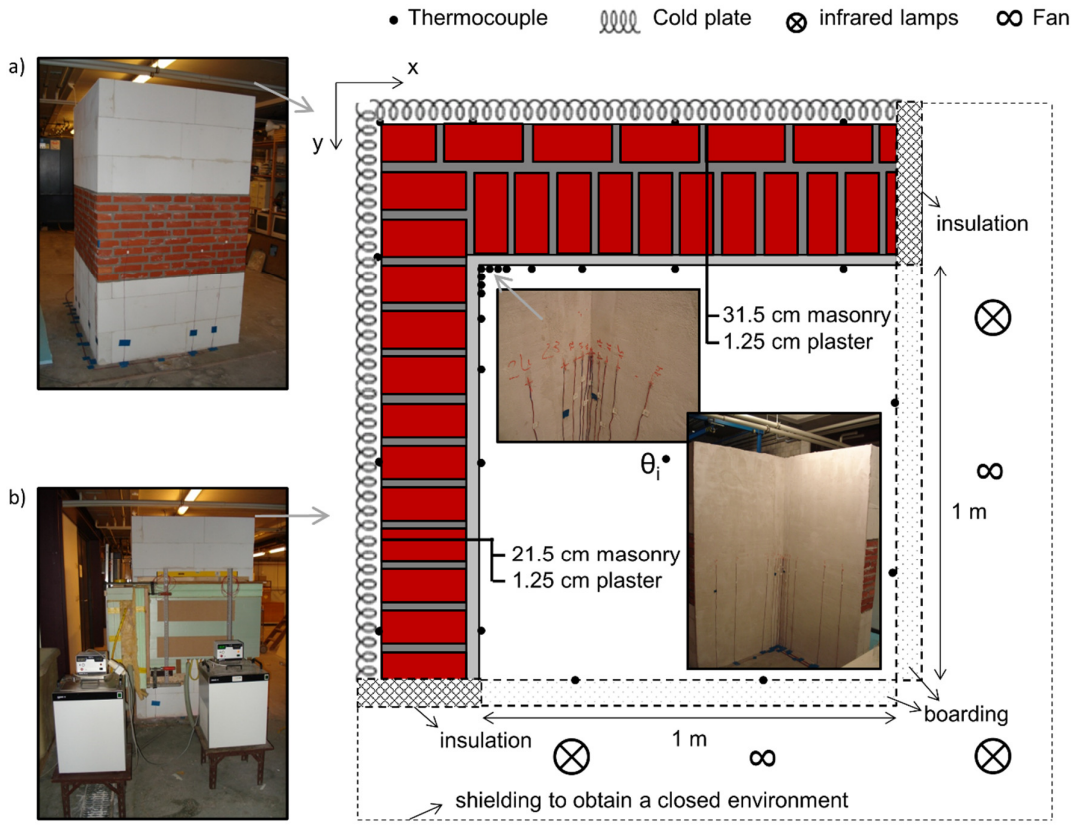

Figure 3. Experimental test setup for Configuration 1 (exterior corner). Inset (a) test setup before the liquid-cooled cold plates were placed, (b) test setup with the liquid-cooled cold plates and the cooling units (before the closed environment was built).

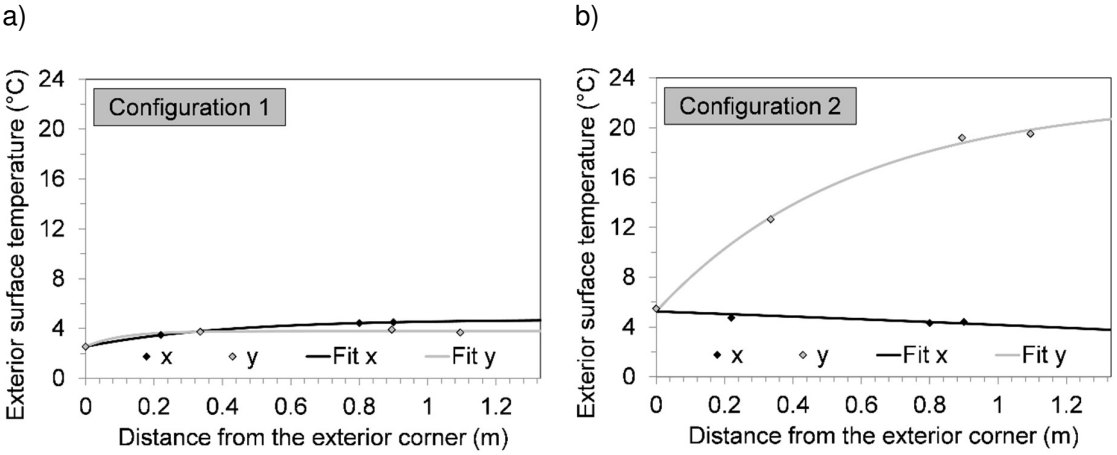

Figure 4. Temperature at the exterior surfaces of the different configurations (see Figure 2). The indices x and y refer to the directions shown in Figure 3. The markers indicate the measurement points.

Boundary conditions

In the different measurements, the configurations were exposed to steady-state conditions. As an example, the proposed methodology was applied to the two configurations shown in Figure 2 which were exposed to an exterior surface temperature of approximately 4°C. The real measured temperatures at the exterior masonry leaf together with the fit through the experimental data are shown in Figure 4. For Configurations 2, the temperatures between the 21 cm thick masonry wall and the exterior insulation board (in the test setup) are shown as well. These temperatures represent the temperatures at the symmetry axis of the configuration.

The results obtained for an exterior surface temperature equal to approximately 8°C and 12°C are reported in Vereecken[65].

Determination of the convective heat transfer coefficient near a corner

The proposed methodology for the determination of the convective heat transfer coefficient near a corner of a thermal bridge (see also Figure 1) was applied to the two thermal bridges shown in Figure 2. As we were mainly interested in the profile near the corner, only the first 80 cm section near the corner was simulated. Besides, further away from the investigated corner, a modified air pattern at the junction between the test wall and the boarding could influence the results. The key component in the procedure was the Monte Carlo analysis wherein the thermal performance of the thermal bridge was simulated with HAMFEM.[3] To do so, a number of input parameters were experimentally determined. The exterior surface temperature profiles measured in the experimental test setup (Figure 4) were imposed as Dirichlet boundary conditions in the simulations. A second input in the simulations was the radiative heat exchange between the interior surface and other surfaces in the environment, which was determined beforehand (Appendix 1). For the interior convective heat transfer, a separate approach was applied. This convective heat exchange was implemented as a Neumann boundary condition, containing the experimentally measured interior air temperature and a convective heat transfer coefficient. For the latter, the Monte Carlo analysis was performed by applying a set

of local interior convective heat transfer coefficient profiles. The course of the local convective heat transfer coefficient was assumed and described by equation (6):

$$h_c(x) = h_c \left[1 - \left(1 - \frac{h_{c,corner}}{h_c}\right) \cdot exp\left(\frac{-k \cdot x}{d}\right)\right] \quad (6)$$

where h_c is the convective heat transfer coefficient away from the corner (W/(m²K)), $h_{c,corner}$ is the convective heat transfer coefficient in the corner (W/(m²K)), k is a parameter defining the slope of the profile (-), d is the wall thickness (m) and x (or y for the second wall surface of the thermal bridge) the distance from the interior corner (m), as shown in Figure 5. Parameters h_c, $h_{c,corner}$ and k in equation (6) were unknown in the Monte Carlo analysis. The convective heat transfer coefficient in the interior corner (x or y = 0) was equal for the x- and y-direction. Hence, for the convective heat transfer coefficient across both wall surfaces, five unknown parameters remained: $h_{c,corner}$, h_{cx}, k_x, h_{cy} and k_y. The output variables in the numerical analysis were the interior surface temperatures. The aim of the Monte Carlo analysis was the inverse determination of the values for the five unknown parameters mentioned above, via minimisation of the summed square error between experimentally and numerically obtained interior surface temperatures. In addition to the parameters describing the profile of the convective heat transfer coefficient, other variables could be included as well in the Monte Carlo analysis. This could be of

interest in cases of an uncertainty on the parameters that describe the test configuration (e.g., material properties and dimensions) or the implemented boundary conditions (e.g., exterior surface temperature and indoor air temperature). In the current study, the heat conductivity of the plaster and the masonry were not accurately known and, thus, were considered as additional unknown parameters in the Monte Carlo analysis. The heat conductivity of the plaster was assumed to lie between 0.5 and 1.5 W/(mK). The minimum and maximum thermal conductivity of the masonry were set at 0.9 and 1.1 W/(mK) respectively, as derived from a complementary heat flux measurement. For the parameters indicating the heat conductivities, a uniform distribution was assumed in the Monte Carlo simulations. The distributions of other input variables in the first Monte Carlo analysis were as follows: $h_{c,corner}$ = U(1,5), h_{cx} = U(2,6), h_{cy} = U(2,6), k_x = U(1,10), k_y = U(1,10), where U(a,b) indicates a uniform distribution between a and b. Although a correlation between the parameters h_c, $h_{c,corner}$ and k is plausible, no correlation was taken into account in the current study. This was primarily because the complex boundary conditions in the test setup (i.e., cooled surface between warmer cellular concrete boards) had complicated a simple reasoning on the air flow pattern in the test room and, hence, boycotts a reliable argumentation of the potential correlations. At the end of the Monte Carlo analysis though, results with $h_{c,corner}$ larger than $h_{c,x/y}$ were discarded. For each Monte Carlo analysis 600 samples were created by use of a

maximin Latin Hypercube sampling scheme.[66] To achieve steady-state conditions, a four-day period was simulated for each run. In the experiment, the measurement data were extracted after achieving steady-state, which was detected by continuously logging the temperatures.

For each of the unknown parameters, its correlation with the summed square error was investigated based on a scatter plot[63]. If a correlation was observed, a new Monte Carlo analysis was performed wherein a smaller interval was applied for the relevant unknown parameter. This iterative process thus allows a reduction of the spread in plausible results for the convective heat transfer coefficient profile. To reduce the required computational time for the Monte Carlo analysis, an advanced sampling technique[64] can be applied.

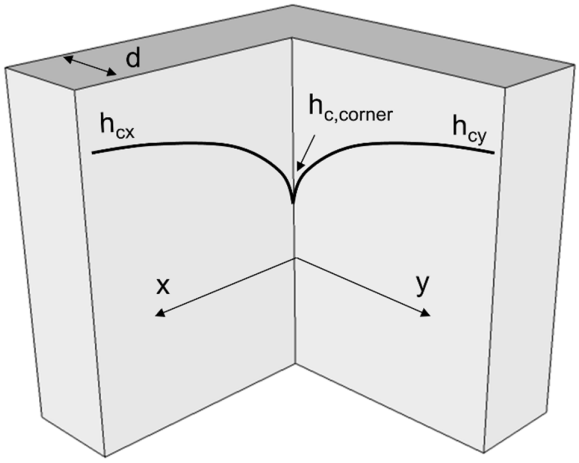

Figure 5. Parameters in equation (6), representing the spatial profile of the convective heat transfer coefficient.

Postprint: Vereecken E, Janssen H, Roels S. 2018. A determination methodology for the spatial profile of the convective heat transfer coefficient on building components. *Indoor and Built Environment 27(4), 512-527*. DOI: 10.1177/1420326X16677330

RESULTS

Air and local interior surface temperatures

The air temperatures (measured with the thermocouple shielded with tin foil) obtained in the test setup were 20±0.8 and 20±0.4°C during the entire measurement duration for Configurations 1 and 2, respectively. By selecting a shorter time period during the steady-state period, the inaccuracy could be reduced to ±0.1°C.

The local interior surface temperature measured in the experiments is shown in Figure 6. The lower temperature at the corner was clearly visible. For the exterior non-insulated wall (Configuration 1), the temperature in the interior edge was much lower compared with the results for Configuration 2. Further away from the corner, a smaller difference between the surface and air temperature occurs for the walls of Configuration 2.

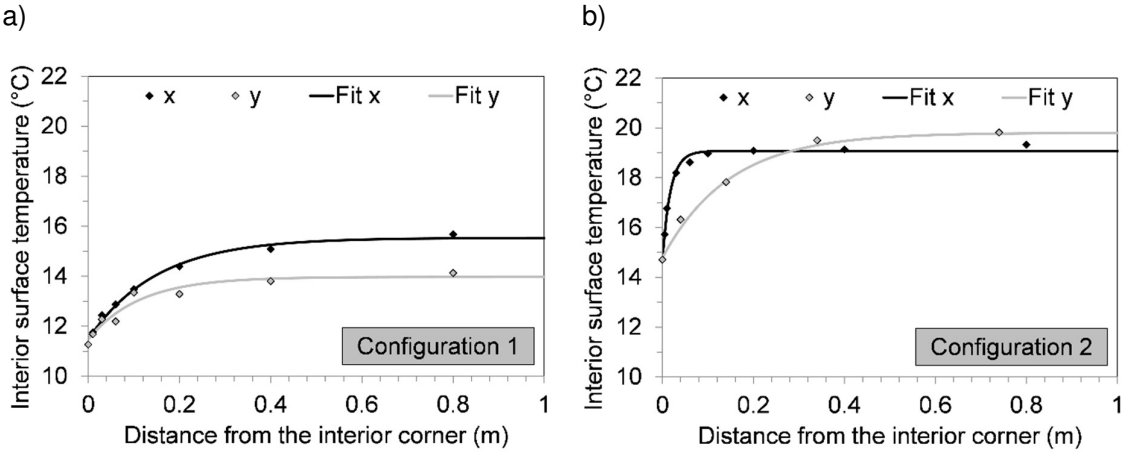

Figure 6. Temperature at the interior surface of the different configurations (see Figure 2). The indices x and y refer to the directions shown in Figure 3. The markers indicate the measurement points.

Radiative heat exchange

The radiative heat exchange was calculated as explained in Appendix 1 and is shown in Figure 7 for the two different configurations. A negative value for the radiative heat exchange implies that the heat transfer was to the surface; the temperatures of enclosing surfaces (boarding, ceiling, floor, cellular concrete layer above and below the masonry layer) were higher than those of the test wall. The interior surface temperature for the 21 cm thick masonry wall (y) of Configuration 1 was lower than for the thicker wall (x), and the radiative heat exchange to the former wall was hence larger. For Configuration 2, further away from the corner, almost no

net radiative heat exchange occurred. Near the corner (where $T_x > T_y$, see Figure 6(b)), the net radiative heat exchange to the exterior wall (x) was smaller than to the interior wall (y).

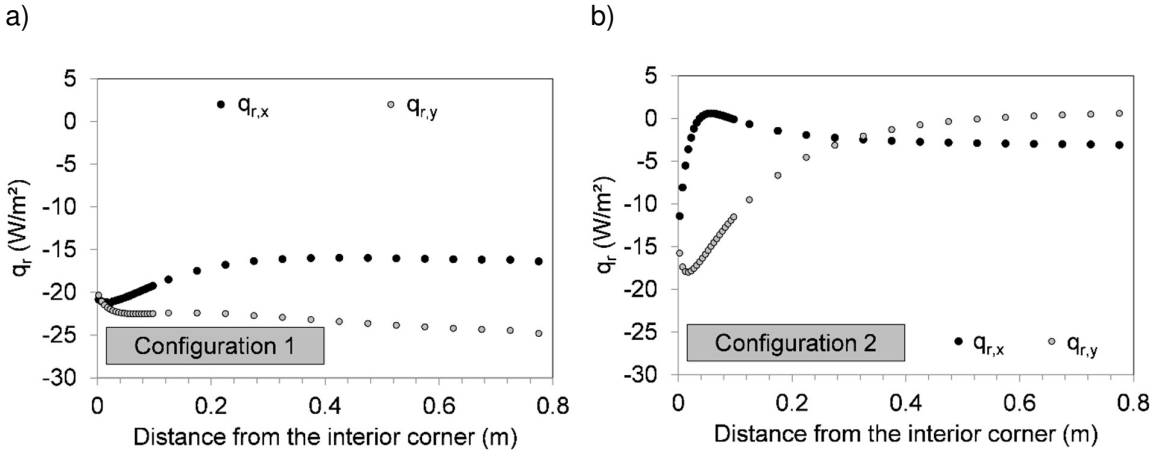

Figure 7. Radiative heat exchange for the two configurations (Figure 2). The indices x and y refer to the directions shown in Figure 3.

Spatial profile of the local convective heat transfer coefficient

To determine the spatial profile of the local convective heat transfer coefficient, the scatter plots for the different unknown parameters in the Monte Carlo analysis were drawn. These plots show the effect of each parameter on the square of the sum of the squared differences between the measured and simulated temperatures, where the square was taken to show a potential minimum more clearly. As an example, Figure 8 shows the scatter plot obtained for h_{cx} for Configuration 1. The plot shows a

minimum in the range between 2.7 and 4.8, indicating a smaller error in this range. Therefore, based on the scatter plot, the search interval for the input variable h_{cx} was reduced. The next Monte Carlo analysis was accomplished with reduced intervals for the unknown parameters, and an iteration was performed until the minimum could no longer be observed in the scatter plots. In this way, the band of plausible output results could be reduced. Figure 9(a) and (b) show the envelopes of the ten convective heat transfer profiles with the lowest summed squared errors (and with $h_{c,corner}$ smaller than $h_{cx/y}$) for the two configurations. Figure 9(a) shows the envelope obtained based on the first and the final Monte Carlo analysis for Configuration 1. Based on the results of the final Monte Carlo analysis, a fairly small spread on the convective heat transfer coefficient was found. The envelopes could provide no information about the combinations for $h_{c,corner}$, $h_{cx/y}$ and $k_{x/y}$. Therefore, the profiles with the lowest (A) and second lowest (B) summed square errors are shown as well.

Postprint: Vereecken E, Janssen H, Roels S. 2018. A determination methodology for the spatial profile of the convective heat transfer coefficient on building components. *Indoor and Built Environment 27(4), 512-527*. DOI: 10.1177/1420326X16677330

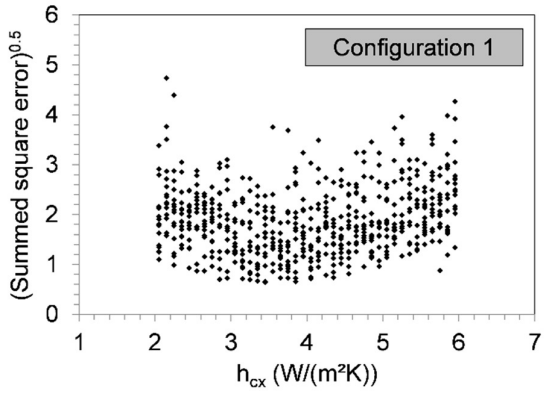

Figure 8. Scatter plot of the first Monte Carlo simulation performed for Configuration 1 (exterior corner, see Figure 2(a)): input variable h_{cx}.

Postprint: Vereecken E, Janssen H, Roels S. 2018. A determination methodology for the spatial profile of the convective heat transfer coefficient on building components. *Indoor and Built Environment 27(4), 512-527*. DOI: 10.1177/1420326X16677330

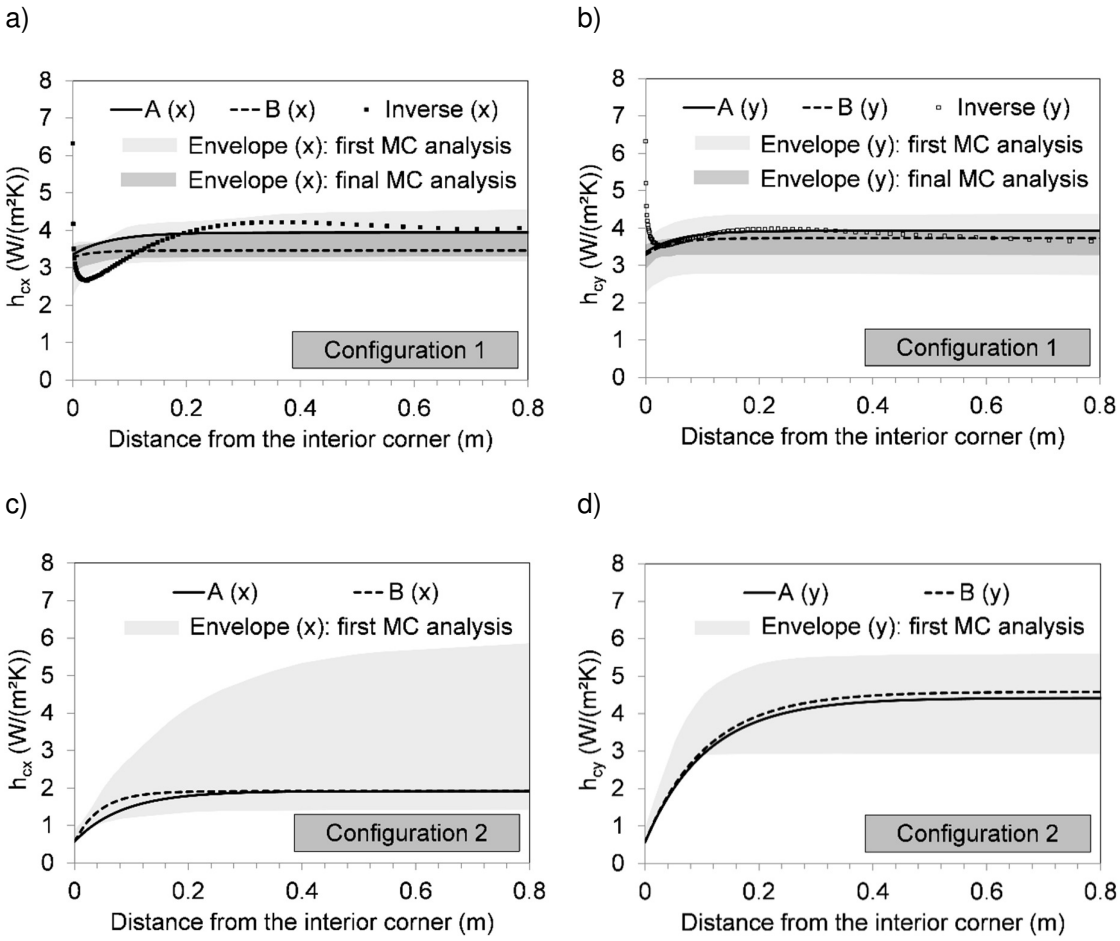

Figure 9. Local convective heat transfer coefficient for the two configurations (see Figure 2). The indices x and y refer to the directions shown in Figure 3. (A, B = course with respectively the lowest and second lowest summed square error). Additionally, for Configuration 1, the profiles obtained based on the inverse determination methodology as applied by Erhorn and Szerman[24] were plotted.

As mentioned in the introductory section, the spatial profile of the local heat transfer coefficient had already been studied by Erhorn and Szerman.[24] The outcome achieved based on their inverse determination methodology is shown in Figure 9(a) and Figure 9(b) as well for Configuration 1 (by square markers). These profiles show a physically unrealistic course near the corner, due to factors such as the inaccuracy of the measured temperature profile in combination with a high numerical sensitivity. However, the convective heat transfer coefficient further away from the corner gives a good indication of the expected magnitude of h_{cx}, h_{cy}.

Since a smaller interval for the input variables did not result in a significant influence on the envelopes for Configuration 2 (Figure 9(c) and 9(d)), only the results of the final Monte Carlo analysis are shown.

For Configuration 2 (Figure 9(c) and 9(d)), the convective heat transfer coefficient in the corner tended to reach the minimum value applied in the analysis. This is clearly visible in the scatter plots as well (see Figure 10). For the convective heat transfer coefficient further away from the corner, a large spread was found. In a second Monte Carlo analysis (not shown), the minimum and maximum convective heat transfer coefficient in the corner were reduced. Additionally, for k_x and k_y, a larger interval was implemented to allow a sufficiently fast increase of the convective heat transfer coefficient. As expected, this resulted in a convective heat transfer in the corner approaching zero. The large spread for the convective heat transfer coefficient

further away from the corner remained. Although a low convective heat transfer coefficient in the corner is plausible, high numerical sensitivity to factors such as the small temperature difference and small measurement inaccuracies could lead to an unreliable result. The small difference between surface and air temperature seems to compromise the applicability of the proposed methodology. Hence, for this boundary condition, the accuracy of the results is questionable.

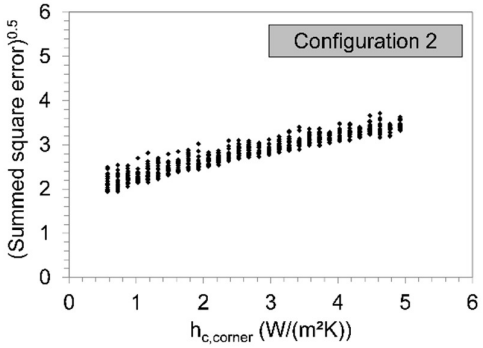

Figure 10. Scatter plot of the first Monte Carlo simulation performed for Configuration 2: input variable $h_{c,corner}$.

DISCUSSION

In this paper a methodology to determine the spatial profile of the local convective heat transfer coefficient was proposed and applied to two thermal bridges. Although the methodology seems promising when comparing the results for Configuration 1, the large spread in results for Configuration 2 indicates that still some improvements

are required. A number of assumptions and simplifications together with the main remarks are discussed below.

Choice of the profile description

For the spatial profile of the convective heat transfer coefficient, the exponential profile described by equation (6) was assumed. This profile was based on the exponential profile for the total heat transfer coefficient near a corner as suggested by Erhorn and Szerman.[24] Given the exponential profile for the total heat transfer coefficient and for the radiative heat transfer coefficient,[65] an exponential profile for the convective heat transfer coefficient is highly plausible as well.

Erhorn and Szerman[24] assumed that the wall thickness could influence the slope of the profile of the local heat transfer coefficient. In the current study, the wall thickness was implemented in the exponential profile for the local convective heat transfer coefficient as well. However, since parameter k in equation (6) was implemented as a variable which can have a different value for the 31.5 cm and the 21.5 cm thick masonry wall, the slope of the profile was not necessarily determined by the wall thickness in the numerical analysis. An overview of parameters $h_{c,corner}$, $h_{cx/y}$, and $k_{x/y}$ for the cases with the lowest and second lowest summed square errors is given in Table 1. For the most appropriate profiles determined in this paper, in general, parameter k_x was different from k_y. Hence, no evidence for the dependency on the wall thickness was found.

For certain cases, other mathematical functions such as a polynomial function could be preferred to describe the profile of the heat transfer coefficients. This is especially true for more realistic cases in which windows or heating systems are present, and for other applications.

Table 1. Overview of the convective heat transfer in the corner ($h_{c,corner}$), the convective heat transfer coefficient away from the corner ($h_{cx/y}$) and the parameter defining the slope of the profile ($k_{x/y}$) determined for the two configurations.

	Lowest summed square error					Second lowest summed square error				
	$h_{c,corner}$	h_{cx}	h_{cy}	k_x	k_y	$h_{c,corner}$	h_{cx}	h_{cy}	k_x	k_y
Configuration 1	3.35	3.94	3.93	5.05	3.85	3.28	3.46	3.73	8.95	5.35
Configuration 2	0.58	1.92	4.42	3.85	2.05	0.58	1.92	4.58	7.15	2.05

Profile selection

The envelopes of plausible convective heat transfer coefficient profiles are defined based on the ten simulations with the smallest summed square errors. Another approach could be to use the profiles with a summed square error lower than a specific value. Due to the difference in summed square error, no general conclusion can be drawn based on the spread in results obtained for the different configurations and exterior surface temperatures.

Sensitivity analysis and literature comparison

In the current study, the measured temperatures were used as exact values. In fact, an inaccuracy was expected due to the thermocouple itself, the fixation of the thermocouple, etc. To show the potential impact of this inaccuracy, an uncertainty analysis was performed for configuration 1 by assuming two worst case scenarios defining the highest positive and negative differences in the flux. To this end, the indoor air temperature and the surface temperature measured at the exterior surfaces, the interior surfaces and the other surfaces in the test environment (resulting in radiative heat exchange) were modified by the positive/negative errors given in Table 2. A patterned error on the thermocouples (e.g., all thermocouples at the interior surface measure a temperature that is 0.1°C higher) and a simultaneous appearance of all the deviations defined in Table 2 are rather unlikely. In this way, the two defined scenarios can definitely be seen as worst case scenarios. The uncertainty of 0.1°C assumed in the analysis was based on the uncertainty of the thermocouples after an individual calibration. As in the current study extra attention was paid to proper positioning of the thermocouples, the additional inaccuracy due to this positioning was assumed of minor importance in our test case. For both scenarios the proposed determination methodology was applied. The envelope achieved based on the lowest (scenario 1) and highest (scenario 2) convective heat transfer profiles (out of the ten convective heat transfer profiles with the lowest

summed square error found for scenarios 1 and 2, respectively) is shown in Figure 11. Additionally, the profiles resulting in the first and second lowest summed square errors in the original study were replotted. An acceptable range on the convective heat transfer profiles was obtained. The order of magnitude of the convective heat transfer coefficients further away from the corner was in agreement with the selection of literature data[10,13,19-22,68-74] shown in Figure 11.

Table 2. Temperature deviations assumed in the two worst case scenarios in the uncertainty analysis

	Exterior surface temperature (°C)	Interior surface temperature (°C)	Indoor air temperature (°C)	Temperature at the other enclosing wall surfaces (°C)
Scenario 1	+0.1	-0.1	+0.1	+0.1
Scenario 2	-0.1	+0.1	-0.1	-0.1

Inaccuracy implementation

The proposed methodology allows a direct implementation of certain inaccuracies. For instance, the noise on the exterior surface temperature or indoor air temperature could be included as an input variable in the Monte Carlo analysis. Furthermore, a

lower and upper experimentally determined interior surface temperature course could be defined based on potential inaccuracies. The simulated temperature course has to fall between this lower and upper course. Parameter sets corresponding to a temperature course that falls outside this lower and upper bound could be penalized in the scatter plots. Recall that when applying the inverse determination method of Erhorn and Szerman,[24] small inaccuracies of the measured interior surface temperature can – especially near the corner – have a significant impact on the spatial profile of the heat transfer coefficient. The indirect way of inaccuracy implementation in the novel methodology presented in the current paper is more flexible and less sensitive to small inaccuracies.

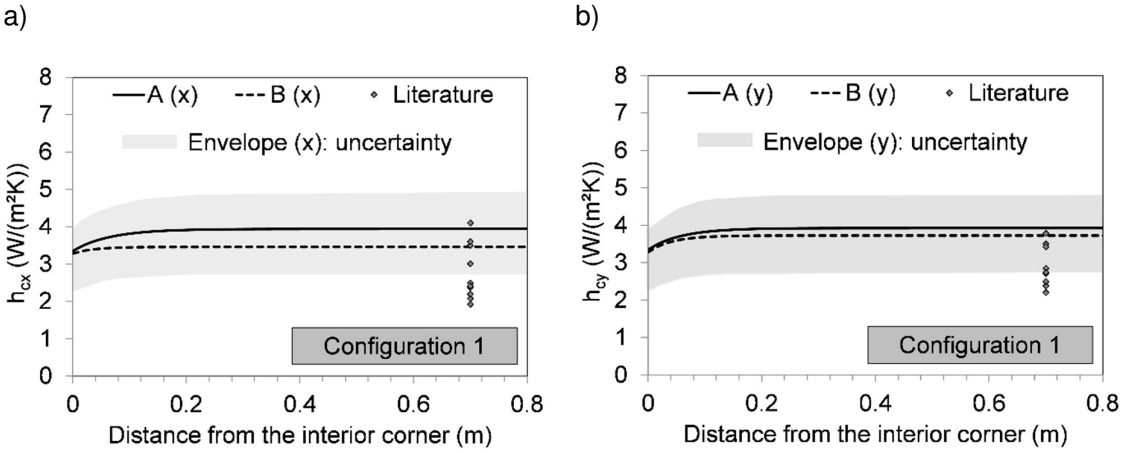

Figure 11. Worst case uncertainty range for the local convective heat transfer coefficient for Configuration 1 (see Figure 2), obtained for the worst case scenarios defined in Table 2. The indices x and y refer to the directions shown in Figure 3. A, B = course with respectively the lowest and second lowest summed square error in the original case. Additionally, a selection of literature data[10,13,19-22,68-74] is shown.

Black box tool

In the current methodology the physical phenomena influencing the convective heat transfer are not entirely included. As shown in Vereecken[65], physically unrealistic profiles for the convective heat transfer coefficient could result in a good agreement between the experimentally and numerically obtained surface temperature. This shows that, to obtain reliable results, the methodology should not be applied as a black box tool.

General validity of results

In the current analysis, the spatial profiles of the local heat transfer coefficient were determined solely for the test setups. Due to the warmer surfaces of the cellular concrete board above and below the cooled masonry strip in these experimental test setups, air movements caused by buoyancy and other forces may have been more pronounced than in real buildings. This could influence the values of the convective heat transfer coefficient. In practice, the heating system, furniture, the air circulation in the room, the surface temperature distribution, etc. could influence the heat transfer coefficient. Hence, the spatial profiles of the convective heat transfer coefficient determined in the current paper, as any experimentally determined heat transfer coefficients, are not generally applicable.

CONCLUSIONS

The brief literature review at the start of this paper showed that the existing measurement procedures for the convective heat transfer coefficient have some drawbacks when one wants to determine the spatial profile of the local convective heat transfer coefficient for building components. Therefore, a methodology based on a combination of experimental work and a Monte Carlo analysis was developed. An advantage of this method is that neither heat flux meters nor artificial heating would be needed. Furthermore, random noise (e.g., uncertainty in configuration and material properties) could be added based on the Monte Carlo analysis.

In this paper, the spatial profile of the local convective interior heat transfer coefficient was determined for (1) an exterior corner, and (2) a junction between an exterior wall with interior insulation and a non-insulated interior wall. The applicability of the proposed methodology was shown for Configuration 1. The convective heat transfer coefficients further away from the corner corresponding to the lowest summed square errors was approximately 4 W/(m²K) for Configuration 1. This value falls in the same order of magnitude as the values obtained based on the method of Erhorn and Szerman and found in other research studies.[13,20-22,68-74] The estimated convective heat transfer coefficient in the corner of Configuration 1 was 3.35 W/(m²K). The estimated values were however determined for a specific case and are hence not generally applicable.

Notwithstanding its applicability for Configuration 1, the proposed method may not be used as a black box tool. For Configuration 2, widely varying results were obtained because of the smaller difference between the surface and air temperatures. Finally, the proposed methodology has the potential to be used in other applications.

AUTHORS' CONTRIBUTION

This study was designed by EV, SR and HJ. Data acquisition was performed by EV. The analysis and interpretation were performed by EV, SR and HJ. The manuscript was written by EV and commented and improved by all authors.

DECLARATION OF CONFLICTING INTERESTS

The authors declare that there is no conflict of interest.

FUNDING ACKNOWLEDGEMENTS

The results in this paper were partially obtained within IWT 3E90050 'Global performance approach and economic analysis of interior insulation with regard to renovation projects' funded by the Flemish Government, KUL OT/09/23 'Towards a reliable application of interior insulation for the retrofit of existing buildings' funded by the KU Leuven and FWO 12J5216N 'Characterisation of hygric properties of building materials via dynamic methods and system identification' funded by FWO-Flanders. These financial supports are gratefully acknowledged.

APPENDIX 1

The total heat flux q_{tot} between a surface and the environment includes a convective (c) and a radiative (r) part, as defined in equation (7):

$$q_{tot} = q_c + q_r \tag{7}$$

As mentioned before, convection and radiation are two different physical phenomena. Hence, a separate approach is required initially. This Appendix

describes the calculation of the radiative heat exchange, which is one of the inputs in the proposed methodology.

Radiative heat exchange is attributed to surfaces with different temperatures. Due to the conservation of energy principle, the net heat transfer from a surface is equal to the net heat transfers from this surface to the other surfaces in the enclosure. For an enclosure with *N* surfaces, the net heat transfer from surface *i* can be described by equation (8):[12]

$$Q_i = \sum_{j=1}^{N} Q_{i\to j} = \sum_{j=1}^{N} A_i F_{i\to j}\left(J_i - J_j\right) \tag{8}$$

where $Q_{i\to j}$ is the heat transfer from surface *i* to surface *j* (W), A_i is the surface area (m²), $F_{i\to j}$ is the view factor and $J_{i/j}$ is the radiosity of surface *i/j* (W/m²). To determine the view factors $F_{i\to j}$, the model developed by Lauzier and Rousse[67] was used. In the determination, the first ten centimetres near the corner were subdivided in elements with a width equal to 5 mm. At a larger distance from the corner (> 10 cm), the mesh width was set to 5 cm. The net heat transfer from surface *i* can also be defined by equation (9) as:[12]

$$Q_i = \frac{A_i e_i}{1 - e_i}\left(\sigma T_i^4 - J_i\right) \tag{9}$$

where e_i is the emissivity of surface i (-), σ = 5.67 x 10^{-8} W/(m²K⁴) and T_s is the surface temperature (K). In the current study, the emissivity was taken as 0.9.

In the calculation of the radiative heat exchange, the surfaces that were taken into account included not only the studied wall surfaces, but also the surfaces above and below the masonry layer, the boarding surface, the floor and the roof. For the local interior surface temperatures on the test walls and the boarding, the temperatures measured by the thermocouples were used, which are shown in Figure 6 for the test wall. For the other wall parts in the test setup a surface temperature of 20°C was assumed. A slightly different surface temperature for these parts was found to have a negligible influence on the determination of the radiative heat exchange.

Combining equations (8) and (9) with the interior surface temperature interpolations (Figure 6) allows the determination of the radiosity of the different subsurfaces and hence of the net heat exchange for each mesh element.

REFERENCES

1. Sharples S. Full scale measurements for convective energy losses from exterior building surfaces. Build Environ 1984;19(1): 31-39.
2. Sharples S, Charlesworth PS. Full-scale measurements of wind-induced convective heat transfer from a roof-mounted flat plate solar collector. Sol Energy 1998;62(2): 69-77.

3. Janssen H, Blocken B, Carmeliet C. Conservative modeling of the moisture and heat transfer in building components under atmospheric excitation. Int J Heat Mass Tran 2007;50: 1128-1140.
4. Hwang SD, Kwon HG, Cho HH. Local heat transfer and thermal performance on periodically dimple-protrusion patterned walls for compact heat exchangers. Energy 2010;35: 5357-5364.
5. Fedorov AG, Viskanta R. Three-dimensional conjugate heat transfer in the microchannel heat sink for electronic packaging. Int J Heat Mass Tran 2000;43: 399-415.
6. Hanreich G, Nicolics J. Measuring the natural convective heat transfer coefficient at the surface of electronic components. IEEE Instrumentation and Measurement Technology Conference. Budapest, Hungary, May 21-23, 2001; 1045-1050.
7. Nishi Y, Gagge AP. Direct evaluation of convective heat transfer coefficient by naphthalene sublimation. J Appl Physiol 1970;29(6): 830-838.
8. Defraeye T, Blocken B, Koninckx E, Hespel P, Carmeliet J. Computational fluid dynamics analysis of drag and convective heat transfer of individual body segments for different cyclist positions. J Biomech 2011;44(9): 1695-1701.

9. Morini GL. Single-phase convective heat transfer in microchannels: a review of experimental results. Int J Therm Sci 2004;43: 631-651.
10. Anon. Condensation and energy. Sourcebook, IEA-exco ECBCS, Report Annex XIV, Vol. 1, Acco, Leuven, 1991.
11. ISO 6946:1996(E). Building components and building elements – Thermal resistance and thermal transmittance - Calculation method. Geneva: International Organization for Standardization, 1996.
12. Cengel YA. Heat Transfer: A Practical Approach. New York, McGraw-Hill, 2003.
13. Hens H. Building physics – Heat Air and Moisture - Fundamentals and Engineering Methods with Examples and Exercises. Berlin, Ernst & Sohn, 2007.
14. Lomas K. The UK applicability study: An evaluation of thermal simulation programs for passive solar house design. Build Environ 1996;31(3): 197-206.
15. Dos Santos GH, Mendes N, Philippi PC. A building corner model for hygrothermal performance and mould growth risk analysis. Int J Heat Mass Tran 2009;52: 4862-4872.

16. Steskens P, Janssen H, Rode C. Influence of the convective surface transfer coefficients on the heat, air and moisture (HAM) building performance. Indoor Built Environ 2009;18(3): 245-256.
17. Hassan K, Mohamed SA. Natural convection from isothermal flat surfaces. Int J Heat Mass Tran 1970;13: 1873-1886.
18. Al-Arabi M, El-Riedy M. Natural convection heat transfer from isothermal horizontal plates of different shapes. Int J Heat Mass Tran 1976;19: 1399-1404.
19. Khalifa A. Natural convective heat transfer coefficient – a review. I. Isolated vertical and horizontal surfaces. Energ Convers Manage 2001;42: 491-504.
20. Awbi H, Hatton A. Natural convection from heated room surfaces. Energ Buildings 1999;30: 233-244.
21. Khalifa A. Natural convective heat transfer coefficient – a review. II. Surfaces in two- and three-dimensional enclosures. Energ Convers Manage 2001;42: 505-517.
22. Wallentén P. Convective heat transfer coefficients in a full-scale room with and without furniture. Build Environ 2001;36(6): 743-751.
23. Abuku M, Janssen H, Roels S. Impact of wind-driven rain on historic brick wall buildings in a moderately cold and humid climate: Numerical analyses of

mould growth risk, indoor climate and energy consumption. Energ Buildings 2009;41: 101-110.

24. Erhorn H, Szerman M. Uberprüfung der wärme- und Feuchteübergangskoeffizienten in Außenwandecken von Wohnbauten. Gesundheits Ingenieur 1992;113(4): 177-232.
25. Crawley DB, Lawrie LK, Winkelmann FC, Buhl WF, Huang YJ, Pederson CO, Strand RK, Liesen RJ, Fisher DE, Witte MJ, Glazer J. EnergyPlus: creating a new-generation building energy simulation model. Energ Buildings 2001;33: 319-331.
26. Crawley DB, Hand JW, Kummert MK, Griffith BT. Contrasting the capabilities of building energy performance simulation programs. Build Environ 2008;43: 661-673.
27. Klein SA, Beckman WA, Mitchell JW, Duffie JA, Duffie NA, Freeman TL, Mitchel JC, Braun JE, Evans BL, Krummer JP, Urban RE, Fiksel A, Thornton JW, Blair NJ, Williams PM, Bradley DE, McDowell TP, Kummert M. 2010. TRNSYS 17 a transient system simulation program, Solar Energy Laboratory, University of Wisconsin, Madison, USA, http://sel.me.wisc.edu/trnsys (2010, accessed 25 Augustus 2016).
28. Awbi H. Calculation of convective heat transfer coefficients of room surfaces for natural convection. Energ Buildings 1998;28: 219-227.

29. Beausoleil-Morrison. The adaptive simulation of convective heat transfer at internal building surfaces. Build Environ 2002;37: 791-806.
30. Fohanno S, Polidori G. Modelling of natural convective heat transfer at an internal surface. Energ Buildings 2006;38: 548-553.
31. Steskens P, Janssen H, Rode C. Evaluation of sub-zonal airflow models for the prediction of local interior boundary conditions – natural and forced convection cases. Indoor Built Environ 2013;22: 395-409.
32. Neale A. A study in computational fluid dynamics for the determination of convective heat and vapour transfer coefficients. PhD Theses, Montreal, Quebec, Canada, 2006.
33. Blocken B, Defraeye T, Derome D, Carmeliet J. High-resolution CFD simulations for forced convective heat transfer coefficients at the façade of a low-rise building. Build Environ 2009;44: 2396-2412.
34. Defraeye T, Blocken B, Carmeliet C. CFD analysis of convective heat transfer at the surfaces of a cube immersed in a turbulent boundary layer. Int J Heat Mass Tran 2010;53: 297-308.
35. Gao NP, Niu JL. CFD study of the thermal environment around a human body: a review. Indoor Built Environ 2005;14(1): 5-16.

36. Loveday DL, Taki AH. Convective heat transfer coefficients at a plane surface on a full-scale building façade. Int J Heat Mass Tran 1996;39(8): 1729-1742.

37. Hagishima A, Tanimoto J. Field measurements for estimating the convective heat transfer coefficient at building surfaces. Build Environ 2003;38: 873-881.

38. Parkhurst DF, Duncan PR, Gates DM, Kreith F. Wind-tunnel modelling of convection of heat between air and broad leaves of plants. Agr Meteorol 1968;5: 33-47.

39. Nakamura H, Igarashi T, Tsutsui T. Local heat transfer around a wall-mounted cube in the turbulent boundary layer. Int J Heat Mass Tran 2001;44:3385-95.

40. Chilton TH, Colburn AP. Mass transfer (absorption) coefficients. Ind Eng Chem 1934;26(11): 1183-1187.

41. Mendes PRS. The naphthalene sublimation technique. Exp Therm Fluid Sci 1991;4: 510-523.

42. Kwon HG, Hwang SD, Cho HH. Measurement of local heat/mass transfer coefficients on a dimple using naphthalene sublimation. Int J Heat Mass Tran 2011;54: 1071-1080.

43. Mortensen LH. Hygrothermal microclimate on interior surfaces of the building envelope. PhD Thesis, BYG-DTU, Lyngby, 2007.

44. Wilkie D, White L. Fuel element heat transfer near dimple braces. Nucl. Engng 1966;11: 596-599.

45. Goldstein RJ, Cho HH. A review of mass transfer measurements using naphthalene sublimation. Exp Therm Fluid Sci 1995;10: 416-434.

46. Neal SBH. The development of the thin-film naphthalene mass-transfer analogue technique for the direct measurement of heat-transfer coefficients. Int J Heat Mass Tran 1975;18: 559-567.

47. Steeman H-J, Janssen A, De Paepe M. On the applicability of the heat and mass transfer analogy in indoor air flows. Int J Heat Mass Tran 2009;52: 1431-1442.

48. Liu Y, Harris DJ. Full-scale measurements of convective coefficient on external surfaces of a low-rise building in sheltered conditions. Build Environ 2007;42: 2718-2736.

49. Hippensteele SA, Russell LM. High-resolution liquid-crystal heat-transfer measurements on the end wall of a turbine passage with variations in Reynolds number. National Heat Transfer Conference 1988, HR Jacobs, ed., ASME, Houston, TX, New York, HTD-96, July 24-27, 1988;3: 443-453.

50. Davies M, Martin C, Watson M, Riain CN. The development of an accurate tool to determine convective heat transfer coefficients in real buildings. Energ Buildings 2005;37: 141-145.

51. Khalifa AJN, Marshall RH. Validation of heat transfer coefficients on interior building surfaces using a real-sized indoor test cell. Int J Heat Mass Tran 1990;33(10): 2219-2236.

52. Delaforce SR, Hitchin ER, Watson DMT. Convective heat transfer at internal surfaces. Build Environ 1993;28(2): 211-220.

53. Irving AD, Dewson T, Hing G, Day B. Time series estimation of convective heat transfer coefficients. Build Environ 1994;29(1): 89-96.

54. Lin M, Wang T. A transient liquid crystal method using 3-D inverse transient conduction scheme. Int J Heat Mass Tran 2002;45: 3491-3501.

55. Rebay M, Arfaoui A, Mebarki G, Ben Maad R, Padet J. Improvement of the pulsed photothermal technique for the measurement of the convective heat transfer coefficient. J Therm Sci 2010;19(4): 357-363.

56. Newton PJ, Yan Y, Stevens NE, Evatt ST, Lock GD, Owen JM. Transient heat transfer measurements using thermochromic liquid crystal. Part 1: An improved technique. Int J Heat Fluid Fl 2003;24: 14-22.

57. Hippensteele SA, Poinsatte PE. Transient liquid-crystal technique used to produce high-resolution convective heat-transfer-coefficient maps. In: Visualization of Heat Transfer Process. 29th National Heat Transfer Conference. Atlanta, Georgia, August 8-11, 1993. ASME, New York, HTD 252, pp.13-21.

58. Kakade VU, Lock GD, Wilson M, Owen JM, Mayhew JE. Accurate heat transfer measurements using thermochromic liquid crystal. Part 1: Calibration and characteristics of crystals. Int J Heat Fluid Fl 2009;30: 939-949.

59. Kakade VU, Lock GD, Wilson M, Owen JM, Mayhew JE. Accurate heat transfer measurements using thermochromic liquid crystal. Part 2: Application to a rotating disc. Int J Heat Fluid Fl 2009;30: 950-959.

60. Abdullah N, Talib ARA, Jaafar AA, Salleh MAM, Chong WT. The basics and issues of thermochromic liquid crystal calibrations. Exp Therm Fluid Sci 2010;34: 1089-1121.

61. Yan Y, Owen JM. Uncertainties in transient heat transfer measurements with liquid crystal. Int J Heat Fluid Fl 2002;23: 29-35.

62. Owen JM, Newton PJ, Lock GD. Transient heat transfer measurements using thermochromics liquid crystal. Part 2: Experimental uncertainties. Int J Heat Fluid Fl 2003;24: 23-28.

63. Hamby DM. A review of techniques for parameter sensitivity analysis of environmental models. Environ Monit Assess 1994;32: 135-154.

64. Janssen H. Monte-Carlo based uncertainty analysis: Sampling efficiency and sampling convergence. Reliab Eng Syst Safe 2013;109: 123-132.

65. Vereecken E. Hygrothermal analysis of interior insulation for renovation projects. PhD Thesis, KU Leuven, Leuven, 2013.

66. Husslage B, Rennen G, Van Dam E, den Hertog D. Space-filling Latin Hypercube design for computer experiments. Optim Eng 2011;12: 611-630.

67. Lauzier N, Rousse D. View factors with GUI. University of Naval. http://www.mathworks.com/matlabcentral/fileexchange/5683-view-factors-with-gui (2003, accessed 1 March 2014)

68. Min T, Schutrum L, Pamelee G, Vouris J. Natural convection and radiation in a panel heated room. ASHRAE Transaction 1956;62: 337-358.

69. Almadari F, Hammond G. Improved data for buoyancy-driven convection in rooms. Build Serv Eng Res T 1983;4(3): 108-112.

70. Wilkes G, Peterson C. Radiation and convection surfaces in various positions. Transactions, ASHVE 1938;44: 513-520.

71. Hell. Grundlagen der Warmeubertragung, 3. Aufl. VDI Verlag, Dusseldorf, 1982.

72. Heidt F, Streppel H. Die Warmebilanz and Wandoberflachen in Raumen mit und ohne Sonneneinstyrahlung. Gesundheitsingenieur 1988;H.2, S.61-67.
73. Nansteel M, Greif R. Natural convection in undivided and partially divided rectangular enclosures. Transactions of ASME, J Heat Transf 1981;103: 623-629
74. ASHRAE. Handbook of fundamentals. New York: ASHRAE, 1981.